Nanoscale

RSC Publishing

PAPER

View Article Online
View Journal | View Issue

Cite this: *Nanoscale*, 2013, **5**, 9404

Thiolate-protected Ag_{32} clusters: mass spectral studies of composition and insights into the Ag–thiolate structure from NMR†

T. Udayabhaskararao, M. S. Bootharaju and T. Pradeep*

Received 11th April 2013
Accepted 23rd July 2013

DOI: 10.1039/c3nr03463a

www.rsc.org/nanoscale

Clusters composed of a 32 silver atom core, protected with thiolates of glutathione (GSH) and *N*-(2-mercaptopropionyl)glycine (MPGH), were synthesized by a solid-state route in milligram scale. They do not exhibit surface plasmon resonance unlike their larger sized nanoparticle analogues but show molecule-like features in absorption and luminescence spectra, falling in the visible window. The compositions $Ag_{32}SG_{19}$ (SG: thiolate of glutathione) and $Ag_{32}MPG_{19}$ (MPG: thiolate of MPGH) were identified from electrospray ionization mass spectrometry (ESI MS). Matrix-assisted laser desorption/ionization mass spectrometry (MALDI MS) was not successful for –SG protected clusters as reported before, but for $Ag_{32}MPG_{19}$ a peak at 6.1 kDa was seen at a threshold laser intensity. This peak shifted to low mass region with increasing laser intensity due to systematic losses of Ag_2S. Further confirmation of the composition $Ag_{32}SG_{19}$ was made using various studies such as XPS and EDAX. One-dimensional (1D) and two-dimensional (2D) NMR spectroscopic investigations of $Ag_{32}SG_{19}$ provided interesting spectral features which indicated the dominant –[SR–Ag–SR]– structural motif. This structural motif as the predominant entity is found for the first time in silver clusters.

Introduction

Quantum clusters (QCs) of noble metals are molecules composed of a few to a hundred metal atom cores – even more in some cases – protected with ligands, especially thiols, and are fundamentally different from their bulk and plasmonic analogues in terms of their optical, electronic, and structural properties.[1–4] In the initial years of study, a mixture of gold QCs with unknown compositions were synthesized by the reduction of Au^{3+} in the presence of glutathione (GSH, the thiolate form is written as SG).[5] These clusters were isolated using the technique of gel electrophoresis and their spectroscopic properties were examined in detail. Molecular formulae of these clusters were later understood as $Au_{10}SG_{10}$, $Au_{15}SG_{13}$, $Au_{18}SG_{14}$, $Au_{22}SG_{16}$, $Au_{22}SG_{17}$, $Au_{25}SG_{18}$, $Au_{29}SG_{20}$, $Au_{33}SG_{22}$ and $Au_{39}SG_{24}$ using mass spectral studies.[6] Subsequently, several new protocols were developed to synthesize these QCs individually, *i.e.* well-defined monodisperse Au_nSR_m.[7–11] Depending on the synthesis conditions, type of protecting ligand, solvent polarity and strength of reducing agent, various monodisperse clusters such as $Au_{25}SR_{18}$, $Au_{38}SR_{24}$ and $Au_{144}SR_{60}$ were synthesized.[12] Size exclusion chromatography was used to detect some of the less prominent clusters such as $Au_{40}SR_{24}$ and $Au_{55}SR_{30,31}$.[13–15] In addition to them, Au_{19},[16] Au_{18}[10] and Au_{20}[17] were also synthesized by controlling the kinetics of the reaction through a slow reduction process. Availability of clusters with known composition, especially crystallization of some of them ($Au_{25}SR_{18}$,[18,19] $Au_{38}SR_{24}$,[20] $Au_{36}SR_{24}$[21] and $Au_{102}SR_{44}$[22]) helped to understand them in greater detail. But corresponding developments have not happened in silver clusters. Although several QCs of silver with known chemical composition such as water soluble Ag_7,[23] $Ag_{7,8}$,[24] and Ag_9,[25] as well as organic soluble $\sim Ag_{140}$[26] and Ag_{280}[27] have been made, the growth of the area is not comparable to that of gold analogues. Recently, there has been rapid progress in this area due to the single crystal analysis of Ag_{14},[28] Ag_{16}[29] and Ag_{32}[29] protected by the combined use of thiolate and phosphine ligands. Analogous to the thiol-protected clusters, they also possess molecule-like behaviour in their optical properties but systematic changes in these properties were not seen due to size and structural differences in cores (such as Ag_6^{4+}, Ag_8^{6+}, and Ag_{22}^{12+}). For example, while Ag_{14} is yellow emissive, Ag_{16} and Ag_{32} exhibit blue emission. Their structures are interesting and provide new insights into the atomic structure of thiolated–Ag QCs in comparison to Au QCs.

In recent years, a variety of methods have been developed to produce stable thiolate-protected silver QCs. Among them is the synthesis through a solid-state route.[25] The time required to produce the desired cluster is substantially less here. High yield

DST Unit of Nanoscience (DST UNS) and Thematic Unit of Excellence (TUE), Department of Chemistry, Indian Institute of Technology Madras, Chennai-600 036, India. E-mail: Pradeep@iitm.ac.in

† Electronic supplementary information (ESI) available: Details of experimental procedures and characterization using UV-vis, luminescence, TEM, ESI MS, XPS, FTIR, XRD of $Ag_{32}SG_{19}$ clusters. See DOI: 10.1039/c3nr03463a

of clusters and easy handling of the reaction made this route novel. It is expected that this protocol opens up a new way for the synthesis of a variety of cluster materials. For example, by varying precursor ratios, reducing agents, temperature and solvents, numerous cluster materials are produced through this route. Here, we report the preparation of thiolated Ag_{32} clusters with two ligands in aqueous phase through this method and their most essential characterization. Assignment of chemical composition was made based on mass spectrometry (MS) including electrospray ionization (ESI) and matrix-assisted laser desorption ionization (MALDI), coupled with elemental analysis and X-ray photoelectron spectroscopy (XPS). We proposed the Ag–thiolate structure of the cluster based on a detailed nuclear magnetic resonance spectroscopic (NMR) study.

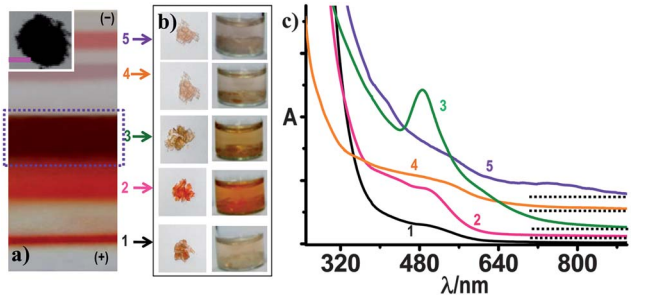

Fig. 1 (a) Distinct bands are seen in the gel, derived from the crude cluster (black powder in inset of a). Scale bar on inset of (a) is 1 cm. (b) Photographs of solidified gel fractions of clusters 1–5 (left) and their water extracts (right). (c) UV-vis absorption spectra of clusters 1–5 extracted from each band after gel electrophoresis of the crude cluster.

Experimental section

Materials and methods

Chemicals. All the chemicals were commercially available and were used without further purification. Silver nitrate ($AgNO_3$, 99%), glutathione (GSH, 97%), *N*-(2-mercaptopropionyl) glycine (MPGH, Aldrich), acrylamide (AR grade), *N*,*N*′-methylenebisacrylamide (BIS) (AR grade), ammonium persulfate and *N*,*N*,*N*′,*N*′-tetramethylethylene diamine (TEMED) were purchased from SRL Chemical Co. Ltd., India. Sodium borohydride ($NaBH_4$, 99.99%, Aldrich), ethanol (HPLC grade, 99.9%, Aldrich) and methanol (HPLC grade) were used as received.

Synthesis of $Ag_{32}SG_{19}$. About 23 mg of $AgNO_3$(s) was added to 200 mg of GSH(s) at room temperature and the mixture was ground well in a mortar to make Ag(I)SG thiolate. About 25 mg $NaBH_4$(s) was added and grinding was continued for 10 more minutes. After that, 10 mL of distilled water was added slowly (in one mL steps) which resulted in the formation of a reddish brown solution. Clusters were precipitated immediately by the addition of excess ethanol. The resulting precipitate was collected and washed repeatedly with ethanol through centrifugal precipitation. Finally, the precipitate was dried and collected as a reddish brown powder (~26 mg). This was termed as crude cluster (CC) in this paper. The dried product was stored in the laboratory atmosphere. Photographs of the synthesis at various stages are shown in ESI, Scheme S1.† The powder was dissolved in water (10 mg mL^{-1}) and kept under ambient conditions overnight. This resulted in a color change from reddish brown to pale pinkish red. This was referred to as aged crude clusters (ACC).

Polyacrylamide gel electrophoresis (PAGE). PAGE was performed using a previously reported procedure.[30] A gel electrophoresis unit with 1 mm thick spacer (Bio-rad, Mini-protein Tetra cell) was used to process the PAGE. The total contents of the acrylamide monomers were 28% (BIS : acrylamide) = (7 : 93) and 3% (BIS : acrylamide) = (7 : 93) for the separation and condensation gels, respectively. The eluting buffer consisted of 192 mM glycine and 25 mM tris(hydroxymethylamine). The crude cluster was dissolved in 5% (v/v) glycerol–water solution (1.0 mL) at a concentration of 10 mg mL^{-1}. The sample solution (1.0 mL) was loaded onto a 1 mm gel and eluted for 4 h at a constant voltage of 150 V to achieve separation as shown in Fig. 1. The gel fractions containing the clusters were cut out, ground, and dipped in ice cold distilled water (2 mL) for 10 min. Subsequently, the solutions were centrifuged at 20 000 rpm for 5 min at −10 °C, followed by filtering with filter paper having 0.22 μm pores to remove the gel lumps suspended in the solution. Separation of cluster 3 was done carefully. For measurements we have cut only the top portion of band 3 (marked in the PAGE photograph) where it is separated far away from the adjacent clusters. Clusters 2 and 3 are merged only at their boundary. Cluster 2 showed as a separate band which indicates that it was not fully mixed with cluster 3. Further PAGE on cluster 3 shows the same UV-vis, luminescence and ESI MS as that of cluster 3.

Synthesis of $Ag_{32}MPG_{19}$. About 23 mg of $AgNO_3$(s) was added to 110 mg of MPGH(s), 1.5 mg of NaOH(s) at room temperature and the mixture was ground well in a mortar to make Ag(I)MPG thiolate. About 25 mg $NaBH_4$(s) was added and grinding was continued for 10 more minutes. After that, 10 mL of distilled water was added slowly (in one mL steps) which resulted in the formation of a reddish brown solution. Clusters were precipitated immediately by the addition of excess ethanol. The resulting precipitate was collected and washed repeatedly with ethanol through centrifugal precipitation. Finally, the precipitate was dried and collected as a reddish brown powder. The powder was dissolved in water (10 mg mL^{-1}) and kept at 10 °C overnight. The resultant solution is called Ag@MPG clusters in the text. Through ESI MS and MALDI MS the composition of the cluster is understood to be $Ag_{32}MPG_{19}$.

Instrumentation. UV-vis spectra were measured with a PerkinElmer Lambda 25 instrument in the range of 200–1100 nm. Luminescence measurements were carried out on a Jobin Yvon NanoLog instrument. The band pass for excitation and emission was set as 2 nm. Circular dichroism studies were measured using a Jasco Model J-810 circular dichroism spectropolarimeter in the range of 200–800 nm. X-ray photoelectron spectroscopy (XPS) measurements were conducted using an Omicron ESCA Probe spectrometer with polychromatic Mg Kα X-rays ($h\nu$ = 1253.6 eV). The samples were spotted as drop-cast films on a sample stub. A constant analyzer energy of 20 eV was used for the measurements. High resolution transmission electron microscopy of clusters was carried out with a JEOL 3010

instrument. The samples were drop-cast on carbon-coated copper grids and allowed to dry under ambient conditions. FTIR spectra were measured with a PerkinElmer Spectrum One instrument. KBr crystals were used as the matrix for preparing samples. ^{1}H NMR were measured with a 500 MHz Bruker Advance III spectrometer operating at 500.13 MHz and equipped with a 5 mm triple-resonance PFG probe. Solutions were made in 99.98% D_2O (Aldrich) and sealed immediately. The signal of the solvent served as the reference for the field-frequency lock. All experiments were performed at a temperature of 25 °C. Standard Bruker pulse programs (Topspin 2.1) were employed throughout. As PAGE purified samples contain tiny quantities of the gel, ^{1}HNMR was performed with the aged crude, which was identical to cluster 3. Mass studies were conducted using an electrospray mass spectrometry (ESI MS) system, LTQ XL (Thermo scientific). Samples of 50 ppm concentration, taken in a 3 : 7 water–methanol mixture, were electrosprayed. Negative ion spectra showed characteristic features in view of the carboxylate species present. Positive ion spectra did not have distinct molecular ion features. Optimized conditions for the negative ion spectra were: capillary temperature: 150 °C, capillary voltage: −34 V, source voltage: −5.7 kV, tubular lens voltage: −110 V and flow rate: 5 μL min^{-1}. Matrix-assisted desorption ionization mass spectrometry (MALDI MS) studies were conducted using a Voyager-DE PRO Biospectrometry Workstation from Applied Biosystems. A pulsed nitrogen laser of 337 nm was used near threshold laser intensity in negative mode. Matrix solution was prepared by dissolving 10 mg of α-cyano-4-hydroxycinnamic acid (CHCA) matrix in a 1 : 1 mixture of acetonitrile (0.5 mL) and trifluoroacetic acid (0.5 mL, 0.1% in DI water). 2 μL of as-synthesized Ag@MPG clusters in water were uniformly mixed with 5 μL of matrix solution. A volume of 2.5 μL of the cluster–matrix mixture was spotted on the target and allowed to dry under ambient conditions. Scanning electron microscopic (SEM) and energy dispersive X-ray (EDAX) analyses were done in a FEI QUANTA-200 SEM. For measurements, samples were drop-cast on an indium tin oxide coated conducting glass and dried in vacuum. Powder XRD patterns of the samples were recorded using a PANalytical X'pertPro diffractometer. The powder samples of parent silver nanoparticles and clusters were taken on a glass plate and the X-ray diffractogram was collected from 5 to 100 degrees in 2 theta using Cu Kα radiation.

Results and discussion

Crude cluster was obtained by grinding the metal precursor and the ligand followed by reduction with $NaBH_4$(s). In this process, initially silver thiolate is formed due to the reaction between $AgNO_3$ and GSH at the interface. High affinity of sulfur to noble metal ions is responsible for thiolate formation which was confirmed from the IR spectrum of the ground mixture, where the S–H_{str} of GSH was absent. Upon addition of sodium borohydride in the solid form, the ground mixture turns to a brownish black powder which shows high affinity to water. At this point, compounds are mixed well, the essential steps of particle formation such as nucleation and growth are controlled due to the lack of protic solvent, which facilitates fast reduction to form metallic particles. This control is important in minimizing the formation of a mixture of clusters compared to solution phase synthesis.

The crude cluster (CC) in water shows an absorption profile different from plasmonic nanoparticles. A peak at 480 nm and shoulders at 550 and 350 nm were observed (Fig. S2a†). Silver clusters protected by glutathione and analogous thiols exhibit distinct features in the region of 300–800 nm.[23–27,30–38] This product, CC, is a mixture of individual silver QCs, as revealed by polyacrylamide gel electrophoresis (PAGE, detailed procedure is in experimental section). Five different bands were separated and are clearly observable on the gel as shown in Fig. 1a. These five bands of different clusters were cut and soaked in ice cold distilled water. Individual clusters were extracted into water, and their distinctive aspects are clearly observable by the appearance of their respective colors. Photographs of the five solid gels and the cluster solutions are given in Fig. 1b. Clusters extracted from these bands are referred to as clusters 1–5, corresponding to the band labels in Fig. 1a. Absorption profiles of all the clusters in water show molecule-like behavior (Fig. 1c). Cluster 5 shows a near-IR absorption peak at 750 nm, along with two other peaks at 540 and 415 nm. Cluster 4 shows a broad peak centered at 550 nm, along with small humps at 350 and 640 nm. Cluster 3 shows a sharp peak 480 nm along with a shoulder peak at 610 nm. Cluster 2 shows distinct peaks at 420, 430 and 490 nm. Cluster 1 shows a broad peak at 490 nm. UV-vis investigations show that the band gaps of these clusters vary with core sizes. A blue shift in the HOMO–LUMO gap with decreasing core size is observed (traces 5 to 1), as seen in gold[6] and silver[31] clusters. The luminescence properties also change in clusters 1–5. Clusters 4 and 5 did not show visible luminescence whereas 2 and 3 exhibit luminescence with maxima at 670 and 680 nm, respectively (Fig. S3†). The shift in luminescence maxima is consistent with the change in cluster size. The yield of CC was ~26 mg, starting from 23 mg of $AgNO_3$. Cluster 3 shows better yield (~15 mg from 23 mg of $AgNO_3$) and stability than the other QCs.

About 10 mg of crude cluster was dissolved in 1.0 mL water and kept under ambient conditions overnight. There was a black precipitate and a clear solution. The precipitate was discarded, which may be due to the decomposition of other metastable clusters. The resultant supernatant is referred to as aged crude cluster (ACC). Aging resulted in a change of color of the solution from reddish brown (CC) to faint pinkish red (ACC) and this change is also reflected in the corresponding powder samples. The powder samples of CC and ACC are black and reddish brown, as shown in insets of Fig. 1a and 2b, respectively.

The absorption spectra of ACC (Fig. S2b†) and cluster 3 (Fig. 1) were similar and therefore, the discarded residue may be due to the decomposition of metastable clusters, 5, 4, 2 and 1. ^{1}HNMR data also support the conversion of a mixture of clusters to a single cluster as there is a reduction in peak width (see later). Features in the circular dichroism (CD) spectrum of ACC matched with its absorption peaks in the 300–700 nm range (Fig. S4†) with strong Cotton signals due to the intrinsic chiral

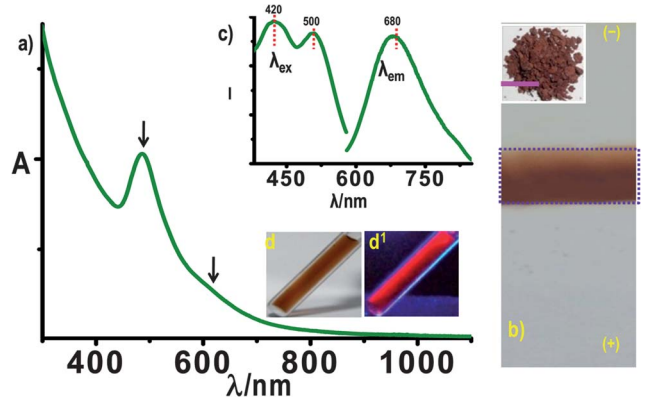

Fig. 2 (a) UV-vis absorption spectrum of the sample in (b). Distinct peaks are marked. (b) Photograph of the PAGE band derived from aged crude. Inset of (b) is the aged crude cluster in powder form. Scale bar on inset of (b) is 1 cm. (c) Excitation and emission spectra of the same. Photographs of this solution in water collected under visible (d) and UV light (d^1).

metal core.[30,33,35,37] It is also noted that the CD signals are in agreement with the glutathione protected silver cluster reported by Kitaev *et al.*[37] The powder obtained after freeze-drying the ACC solution was subjected to PAGE, which showed the presence of a single band (Fig. 2b) whose absorption and luminescence profiles (Fig. 2a† and inset c, respectively) match perfectly with those of cluster 3 (both the bands exhibiting the same mobilities are marked with dotted boxes in Fig. 1a and 2b, respectively). Absorption spectral features of cluster 3 and Ag@SG clusters from the literature[25,31,37] are comparable (Fig. S5†). All of them show similarities in the sharp and shoulder peaks at ~480 and ~610 nm, respectively. The cluster solution exhibits luminescence in the red region, photographs of the solution under visible and UV light are shown in insets d and d^1, respectively, in Fig. 2. Interestingly, the absorption spectrum of recently crystallized Ag_{32} cluster[29] also exhibits a strong peak at 485 nm and a weak peak at 600 nm along with a few additional structures at 450 and 750 nm; the latter two are absent in our present system. Also the crystallized cluster[29] exhibits blue emission but the present system is red emitting. These differences in the optical properties of the systems may be due to the ligand-dependent structural changes. It has to be noted that the ligand 1,2-bis(diphenylphosphino)ethane (DPPE), useful to join tetrahedrally coordinated shell-Ag atoms of the Ag_{22}^{12+} core, is absent in the present system.

The cluster was characterized with various tools as well. As ACC, its PAGE-purified product and cluster 3 gave identical results; the former was used for most of the studies, unless noted otherwise. The cluster responsible was identified as $Ag_{32}SG_{19}$ and the details will be discussed below.

It is worth noting that there are some minor differences in the absorption spectra of ACC and the PAGE-purified product (cluster 3). However, absorption profiles of the PAGE product of ACC (Fig. 2a) and cluster 3 (Fig. 1, trace 3) are the same. An extra peak was observed at 420 nm in ACC (Fig. S2†) and not in the PAGE purified products. Although there is this difference, the excitation and emission spectra for all the clusters are the same (Fig. S3† and 2c). This difference in the absorption spectra is due to the difference in pH of the solutions. Absorption profiles of these clusters show slight changes with pH. The 420 nm peak in ACC at pH 4.2 was absent at pH 6.0. The running gel in electrophoresis is maintained at pH 8.8, and this results in a change in pH after PAGE. Another important aspect to mention is that the 420 nm band of the excitation spectrum of ACC (Fig. 2c) resembles the UV-vis spectrum, indicating that this peak is part of the absorption spectrum and is not due to another cluster. These aspects indicate that they are the same chemically.

Although crystallography is needed for complete characterization, most of the information on the composition of QCs is available from mass spectrometry.[4,6] It is also important to note that –SG protected clusters are difficult to crystallize and crystal structures of none of them have been available till now. The chemical compositions of –SG protected gold clusters were understood solely based on ESI MS.[6] Unlike in the case of gold QCs, obtaining quality ESI MS of silver clusters is difficult due to their poor stability. In most cases, the ESI conditions, especially the capillary and transfer tube temperatures, cause decomposition of the clusters. As a result, only a few Ag QCs with known composition exist up to now. Most of the studies of these clusters are limited to understanding their optical properties,[30,33–37,39] and applications in sensing.[40–42]

Negative ion ESI MS of cluster 3 and aged cluster in a water : methanol mixture yield the same ESI MS data. The spectra are composed of a series of multiply charged anions originating from deprotonation of the carboxyl moieties of the –SG ligands as it is a dicarboxylic acid. It can undergo two ionizations, but in the pH of the cluster solution (~4.2), a monoanion $(SG–H)^-$ is preferred. However, –SG ligand can also

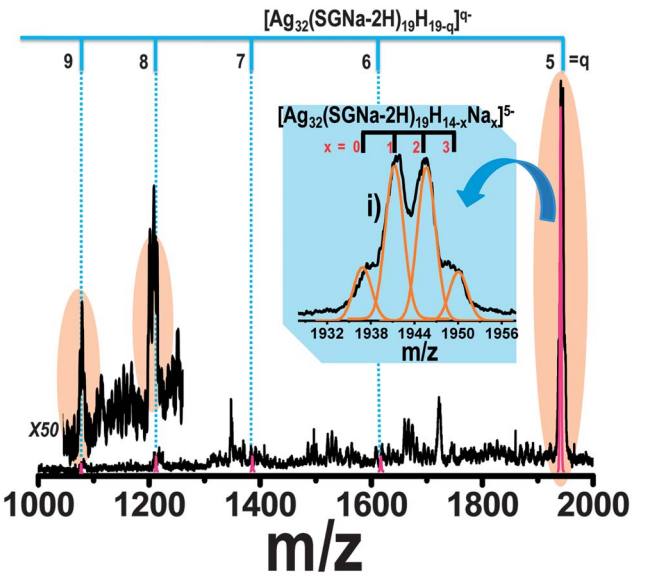

Fig. 3 ESI MS of $Ag_{32}SG_{19}$ in negative mode in the range of m/z 1000–2000. Calculated positions corresponding to the multiply charged species (5^- to 9^-) of $[Ag_{32}(SGNa\text{-}2H)_{19}H_{19-q}]^{q-}$ are shown on the top of the spectrum. Pink colored peaks correspond to the calculated peaks positions of $[Ag_{32}(SGNa\text{-}2H)_{19}H_{19-q}]^{q-}$. Inset (i) is a comparison of the calculated and experimental spectra of $[Ag_{32}(SGNa\text{-}2H)_{19}H_{14-x}Na_x]^{5-}$, where $x = 0$, 1, 2 and 3.

exist as a sodium salt and therefore the monoanion formed may be represented as $(-SGNa\text{-}2H)^-$. As there are multiple SG ligands, there are a number of such species.

Cluster 3 shows a series of peaks in the range of *m/z* 1200–2500 (Fig. 3). However, it is quite difficult to understand the peaks due to the complexity of the spectrum. Recently, Griffith *et al.*[43] reported the mass spectrum of $Ag_{32}SG_{19}$, isolated from gel electrophoresis of crude clusters. The absorption profile of this cluster matches well with our cluster (Fig. S5†). But, the mass spectral series obtained by Griffith *et al.* is different from our study. This discrepancy may be due to the synthesis protocol which adds sodium ions in our case and also due to instrumental variations. The calculated multiply charged peaks for $[Ag_{32}(SGNa\text{-}2H)_{19}H_{19-q}]^{q-}$ are matching well with the ESI MS data [note: $Ag_{32}(SGNa\text{-}2H)_{19}H_{19}$ is the parent neutral molecule]. For example, a highly intense peak centred at *m/z* 1941 corresponds to $[Ag_{32}(SGNa\text{-}2H)_{19}H_{14}]^{5-}$. Upon close observation we find that the peak is composed of four peaks at *m/z* 1936 $[Ag_{32}(SGNa\text{-}2H)_{19}H_{14}]^{5-}$, *m/z* 1941 $[Ag_{32}(SGNa\text{-}2H)_{19}NaH_{13}]^{5-}$, *m/z* 1945 $[Ag_{32}(SGNa\text{-}2H)_{19}Na_2H_{12}]^{5-}$ and *m/z* 1949 $[Ag_{32}(SGNa\text{-}2H)_{19}Na_3H_{11}]^{5-}$ (inset i, Fig. 3). Such sodium additions are common in cluster mass spectrometry.[23,25] Similarly, mass spectral peaks corresponding to $[Ag_{32}(SGNa\text{-}2H)_{19}H_{19-q}]^{q-}$ also appeared at the calculated positions, where *q* is the overall charge of the cluster (6, 7, 8 and 9). For example, the peaks due to $[Ag_{32}(SGNa\text{-}2H)_{19}H_{13}]^{6-}$, $[Ag_{32}(SGNa\text{-}2H)_{19}H_{12}]^{7-}$, $[Ag_{32}(SGNa\text{-}2H)_{19}H_{11}]^{8-}$ and $[Ag_{32}(SGNa\text{-}2H)_{19}H_{10}]^{9-}$ are at *m/z* 1617, 1386, 1212, and 1078, respectively. Although the calculated positions match well, the resolution at these charge states is not adequate to see the isotope pattern of silver. The peaks are quite broad and several other peaks surround the main peak. This complication is due to the presence of sodium adducts. The other complication corresponds to a cleavage of the amide bond between glutamic acid and cysteine, a fragmentation process commonly observed in glutathione, as evidenced by its presence in the tandem mass (mass spectrometry/mass spectrometry, MS/MS) spectrum of glutathione itself (Fig. S6†). This kind of fragmentation is also observed for glutathione protected gold clusters.[10] ESI MS in the range of *m/z* 400–1200 shows low mass region peaks at *m/z* 936, 828, 522 and 414 assigned to $[Ag_3SG_2\text{-}H]^-$, $[Ag_2SG_2\text{-}H]^-$, $[Ag_2SG\text{-}H]^-$ and $[AgSG\text{-}H]^-$, respectively (Fig. S7†). We measured the mass spectrum of the well-known cluster, $Au_{25}SG_{18}$ under these conditions and the expected spectrum was seen (Fig. S8†), which confirms the accuracy of the data.

In view of the poorly resolved peaks in the ESI MS data, we wanted to have additional information on the composition of the cluster using other methods. The best option is to compare the results with another soft ionization technique. MALDI MS of the cluster was not successful for further confirmation of the assignment. Note that so far there is no report of the MALDI MS of intact clusters protected with glutathione. In order to obtain both MALDI MS and ESI MS, we tried to synthesize a cluster having the same core with ligands such as cysteine, mercaptosuccinic acid and *N*-(2-mercaptopropionyl)glycine. Among them, the cluster protected with *N*-(2-mercaptopropionyl) glycine (MPGH; its thiolate is labeled as MPG) was selected for further study as its absorption profiles matched exactly with

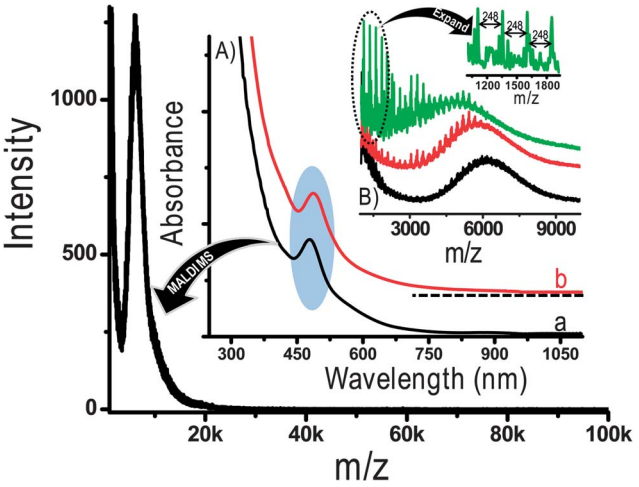

Fig. 4 MALDI MS of Ag@MPG in negative mode. (A) UV-vis absorption spectra of Ag@MPG (a) and $Ag_{32}SG_{19}$ (b) clusters at pH 6.0. (B) Laser dependent MALDI MS spectra of the Ag@MPG cluster at near threshold intensity (black trace, ~1700) and at higher laser intensities (red and green traces). Inset of B show the expanded region of MALDI MS at high laser intensity (~3500).

cluster 3 ($Ag_{32}SG_{19}$). The cluster also gave acceptable MALDI and ESI MS features. We present these data below.

MPG protected Ag QCs (Ag@MPG) were synthesized using the same method used for $Ag_{32}SG_{19}$ (see Experimental section). Precipitate of clusters was taken in 10 mL distilled water and kept for aging at 10 °C. The pH of the resultant solution was 6.0. It showed a sharp peak at ~480 nm and a shoulder around ~600 nm in its absorption profile (inset of Fig. 4). At the same pH, $Ag_{32}SG_{19}$ also shows the same absorption spectrum. The similarity in absorption profiles of these clusters proves that both have the same cluster core. In the case of the luminescence spectrum, there is a slight shift (10–15 nm) in the emission peak position. Unlike in the case of $Ag_{32}SG_{19}$, these clusters do not show visible luminescence under UV light illumination, indicating very low quantum yields compared to glutathione protected ones. It is known that –SG protected Au_{25} shows higher quantum yield compared to other thiols.[44] It is attributed to the electron donating capability (of –SG) due to the presence of electron rich groups (*e.g.*, carboxylic and amino groups). In the case of MPG, the smaller number of electron rich groups made the system have lower quantum yield. Ag@MPG clusters exhibit a single emission at 700 nm when excited at 470 and 540 nm (Fig. S9†). However, there is a slight shift in excitation and emission positions of the clusters ($Ag_{32}SG_{19}$ and Ag@MPG). Note that ligands play an important role in the luminescence profile.[8,44]

This cluster was subjected to MALDI MS using CHCA as the matrix. Negative ion mode MALDI MS (Fig. 4) at threshold laser power (~1700) shows a peak maximum at ~6.1 k. No cluster other than the species giving the 6.1 k maximum was present in the sample. The peak was quite broad compared to the calculated peak and also in comparison to typical MALDI MS data of Au clusters.

Upon closer observation, the 6.1 k peak is composed of peaks spaced at *m/z* 248, especially on the left of the peak, suggesting progressive loss of Ag_2S. Thus, even at threshold laser intensity,

selective fragmentation occurs. The loss of Ag-MPG thiolates is unlikely, which would have given a much larger spacing of *m*/*z* 270. This loss is reflected in the experimentally observed mass spectral position (6.1 k) while the calculated peak position for $Ag_{32}MPG_{19}$ is 6.5 k which was confirmed by ESI MS (see below). We conclude that the alkyl chains are partially dissociated (~3 alkyl groups (~0.13 kDa for each); 6.5–6.1 kDa = 0.4 kDa) from the cluster core during ionization, which also explains the increased peak width. Indeed, loss of alkyl chains by carbon–sulfur (C–S) bond cleavage is common in monolayer protected clusters of gold and silver. The peak at 6.1 k is increasingly shifted towards the low mass region with increasing laser intensity and the spectrum is dominated by a series of peaks separated by *m*/*z* 248 due to Ag_2S loss indicating the loss of a major portion of the alkyl chains (inset of Fig. 4B). By the use of a more optimized matrix, this fragmentation may be avoided. It is important to note that an optimized matrix such as *trans*-2-[3-(4-*tert*-butylphenyl)-2-methyl-2-propenylidene]malononitrile (DCTB) is essential for a high quality mass spectrum of $Au_{25}PET_{18}$.[4]

The Ag@MPG clusters were also subjected to ESI MS. Fig. 5 shows the negative ion (ESI) mass spectrum of Ag@MPG clusters in a water : methanol mixture. MPG is a monocarboxylic acid and its ionization by the loss of H^+ results in $(MPG\text{-}H)^-$. A series of multiply charged species were observed in the mass spectrum of the cluster due to $[Ag_{32}(MPG\text{-}H)_{19}Na_xH_{19-x-q}]^{q-}$, where $q = 3$, 4 and 5. The multiply charged peaks are quite broad due to the addition of sodium ($x = 8$, 9 and 10). Just as in the case of –SG, half the carboxylate functional groups contain sodium. For example, the peak at *m*/*z* 2254 (due to the triply charged species) is due to the merging of peaks corresponding to $[Ag_{32}(MPG\text{-}H)_{19}Na_8H_8]^{3-}$, $[Ag_{32}(MPG\text{-}H)_{19}Na_9H_7]^{3-}$ and $[Ag_{32}(MPG\text{-}H)_{19}Na_{10}H_6]^{3-}$ (inset of Fig. 5). However, there is complexity in the data (extra peaks in the spectrum labeled with *) which may be superimposition of other charged species or other possible fragmentations. In order to understand the system in detail, an improved mass spectrum is required. This is difficult in view of the multiply charged species, although we are continuing our efforts. Peaks of other charges, $[Ag_{32}(MPG\text{-}H)_{19}Na_8H_7]^{4-}$ and $[Ag_{32}(MPG\text{-}H)_{19}Na_8H_6]^{5-}$, were also seen with good intensity. Even at low capillary temperatures, clusters undergo fragmentation resulting in peaks in the low mass region. These fragment peaks appeared with characteristic mass spacing due to silver isotopes, *i.e.* *m*/*z* 2. These peaks at *m*/*z* 1080 and 1188 correspond to $[Ag_4MPG_4\text{-}H]^-$ and $[Ag_5MPG_4\text{-}H]^-$, respectively. These peaks and their sodium adducts are labeled in Fig. 5. The intense peak at *m*/*z* 1902 in the mass spectrum corresponds to the triply charged sodium salt of $Ag_{27}MPG_{16}$, derived from the loss of silver thiolates ($[Ag_5MPG_3\text{-}H]$, which appeared in the low mass region, shown in orange color), from its parent ion, $[Ag_{32}(MPG\text{-}H)_{19}Na_8H_8]^{3-}$. The expanded spectrum of $[Ag_5MPG_3\text{-}H]^-$ is given in Fig. S10.† Based on the agreement between the experimental and calculated peaks, the composition of Ag@MPG clusters is confirmed as $Ag_{32}MPG_{19}$.

The monolayer binding in $Ag_{32}SG_{19}$ through thiolate is supported by XPS (Fig. S11†) and FTIR spectroscopy (Fig. S12†). The XPS survey spectrum shows all the expected elements. The Ag 3d peak is close to an Ag(0) value of 368.0 eV. Note that there is not much difference in the binding energy between Ag(0) and Ag(I) states. The S $2p_{3/2}$ peak is thiolate-like with an observed value of 162.0 eV (Fig. S11c†). This is in agreement with the IR spectrum (Fig. S12†), which suggests the loss of thiolate proton upon cluster formation. From EDAX, the Ag : S atomic ratio measured is 1 : 0.56 ± 0.03 which matches with the expected value of 1 : 0.59 for $Ag_{32}SG_{19}$ (Fig. S13†). A broad peak centered around $2\theta \approx 38°$ in the X-ray diffraction (XRD) pattern is seen, as in the case of Au or Ag QCs,[17,24,25] which shows the absence of metallic nanoparticles (Fig. S14†). The clusters appear as tiny dots in TEM with a size of ~1.0 nm (Fig. S15†).

A recent breakthrough in metal cluster research is the structure determination of $Au_{102}SR_{44}$ followed by those of $Au_{25}SR_{18}$ and $Au_{38}SR_{24}$. Although the "divide and protect" concept (metal core with neutral atoms protected by metal thiolate) was proposed theoretically by Hakkinen *et al.*[45] on $Au_{38}(SR)_{24}$, an understanding of this kind of clusters has taken place only after the above structural data. In $Au_{102}SR_{44}$,[22] the inner core of the cluster contains 79 Au atoms (which are all in neutral state) protected by nineteen $-[RS_C\text{–}Au\text{–}S_CR]-$ and two $-[RS_C\text{–}Au\text{–}S_B(R)\text{–}Au\text{–}S_CR]-$ units, where $(R)S_B$ and RS_C correspond to bridging and core-attached thiolates, respectively. $Au_{38}SR_{24}$[20] contains a face-fused biicosahedral Au_{23} core capped by three $-[RS_C\text{–}Au\text{–}S_CR]-$ and six $-[RS_C\text{–}Au\text{–}S_B(R)\text{–}Au\text{–}S_CR]-$ units. In the case of $Au_{25}SR_{18}$, there are two types of ligands, 6 bridging and 12 core-attached thiolates.[19] The whole entity may be represented as $Au_{13}[RS_C\text{–}Au\text{–}S_B(R)\text{–}Au\text{–}S_CR]_6$. The occupancy of $-[RS_C\text{–}Au\text{–}S_CR]-$ and $-[RS_C\text{–}Au\text{–}S_B(R)\text{–}Au\text{–}S_CR]-$ in Au_{102}, Au_{38}, Au_{25} is 19 : 2, 3 : 6, and 0 : 6. From these observations, as

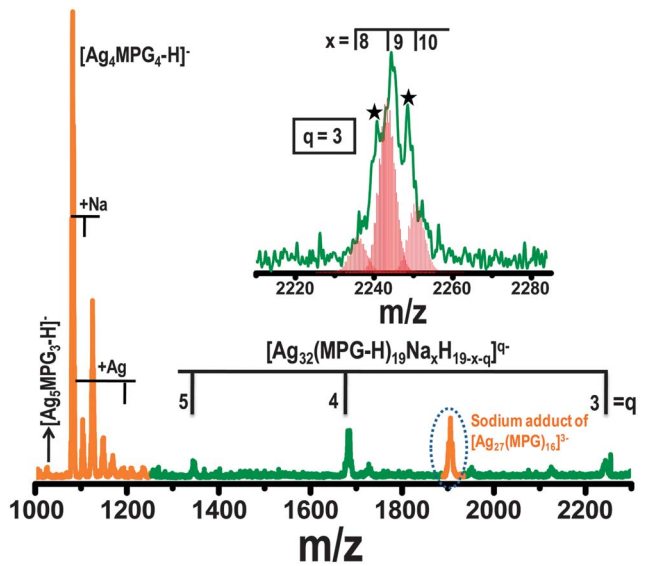

Fig. 5 ESI MS of $Ag_{32}MPG_{19}$ in the negative mode in the range of *m*/*z* 1000–2300. Calculated positions corresponding to the multiply charged species of $[Ag_{32}(MPG\text{-}H)_{19}Na_xH_{19-x-q}]^{q-}$, where $q = 3$, 4 and 5 (shown on the top of the spectrum). Inset shows a comparison of the calculated and experimental spectra of species with $x = 8$, 9, 10 and $q = 3$. These species are $[Ag_{32}(MPG\text{-}H)_{19}Na_8H_8]^{3-}$, $[Ag_{32}(MPG\text{-}H)_{19}Na_9H_7]^{3-}$ and $[Ag_{32}(MPG\text{-}H)_{19}Na_{10}H_6]^{3-}$. The fragments, $[Ag_{27}(MPG\text{-}H)_{16}]^{3-}$ and the Ag thiolates are shown in another color.

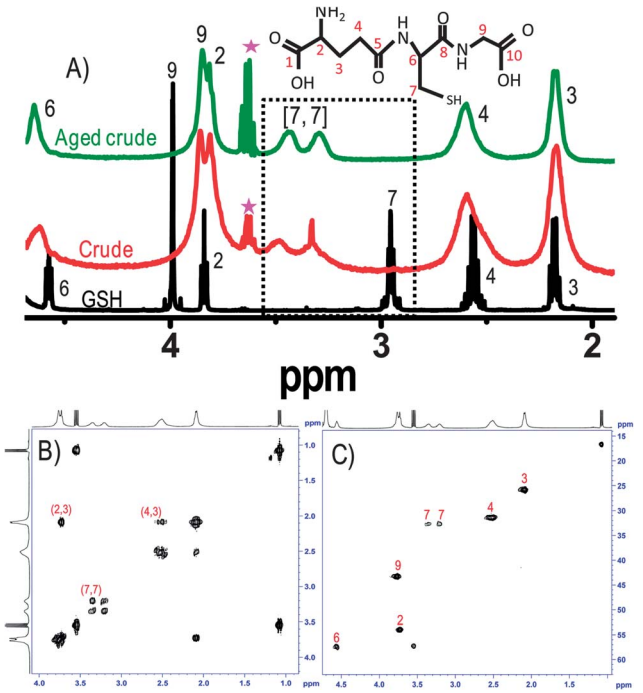

Fig. 6 (A) ^{1}H NMR spectra of GSH, crude cluster and aged crude. The peaks in the dotted box are due to H-7. Peaks at ~3.6 ppm (marked with *) are due to residual EtOH. 2D NMR spectra of $Ag_{32}SG_{19}$ clusters. (B) COSY spectrum. (C) HSQC spectrum. Solvent: D_2O. Note that the CH_3CH_2 signal (^{1}H: 1.1 and 3.6 ppm, ^{13}C: 15.2 and 58.0 ppm) in COSY and HSQC spectra is from residual CH_3CH_2OH. COSY showed the coupling information from the cross peaks. [4,3] and [2,3] protons are coupled together as understood from their cross peaks, marked in (B). H-7 also produces cross peaks without coupling with other sets of protons. In (C), H-7 protons show two signals at 3.2 and 3.5 ppm originating from the same carbon (C-7, 32.0 ppm), due to two hydrogen atoms on C-7.

the size of the core increases to 102, the structure is dominated by –[RS_C–Au–S_CR]–[19,22] while in the smaller clusters, –[RS_C–Au–S_B(R)–Au–S_CR]– units dominate.

Apart from crystal structure studies, NMR can also be used to study the Au-thiolate structure effectively.[8,46,47] For example, independent NMR studies revealed the presence of two kinds of sulfur environments in 2 : 1 ratio (where 2 RS_C : 1 S_BR) in $Au_{25}SR_{18}$.[46,48] Motivated by the recent developments and our own earlier studies,[8] we performed NMR analysis of $Ag_{32}SG_{19}$. It reveals that the structure of the thiolated cluster is quite different from the phosphine analogue.[49] The presence of the inner core and outer shell with metal thiolate is understood from a detailed analysis of NMR.

^{1}H NMR data of the cluster are presented in Fig. 6. Chemical shifts for H-3, H-4, H-2, H-9, and H-6 of glutathionate (–SG) in $Ag_{32}SG_{19}$ are 2.17, 2.60, 3.81, 3.87, and 4.64 ppm, respectively (Fig. 6A, refer to the structure for peak assignments). Protons H-7 (= 3CH–CH_2–S–) signals are significantly shifted downfield in the range of 3.2–3.5 ppm with broadening followed by splitting, noted as [7,7] in Fig. 6A. Downfield shift of H-7 can be understood in terms of its close proximity to the silver core. To know the cause of splitting and nature of the staple motif on the cluster surface in comparison to the structures presented above, homonuclear correlation spectroscopy (COSY) and heteronuclear single quantum correlation (HSQC) were performed (Fig. 6B and C, respectively).

The two-dimensional (2D) NMR data of Ag_{32} clearly rule out complete protection of the core by –[RS_C–Ag–S_B(R)–Ag–S_CR]– units which would have resulted in two pairs of peaks at 2 : 1 ratio for –S_CR and –S_BR, respectively. It is to be noted that the two peaks in a pair correspond to two hydrogen atoms on the 7th position of glutathione. But, we have seen only one pair of peaks, labeled [7,7], which are in 1 : 1 ratio. The presence of the 1 : 1 intensity ratio indicates that all the thiolates are in equivalent environments. Based on the Au–thiolate structure of gold clusters, one can see that the –[S_C–Ag–S_C]– unit alone possesses equivalent thiolates. These results suggest that the Ag–thiolate structure for $Ag_{32}SG_{19}$ is dominated by –[RS_C–Ag–S_CR]–. However, complete protection of –[RS_C–Ag–S_CR]– is also not possible due to the presence of an odd number of ligands (19 SR). It suggests the presence of other Ag–thiolates. But peaks corresponding to them are not detected in NMR, indicating that they are few in number. From the theoretical study of Xiang *et al.*[50] and Balasubramanian *et al.*,[51] we know that –[RS–Ag–RS]– is a stable structural motif for a thiolate-protected Ag QCs. To the best of our knowledge, this is the first experimental evidence for the –[RS–Ag–RS]– structural motif in thiolated Ag QCs. It is in contrast to Au_{25} and Au_{38} clusters, where NMR study reveals that they are dominated by –[RS_C–Au–S_B(R)–Au–S_CR]–.

Summary and conclusions

In summary, we have synthesized –SG protected Ag_{32} clusters. Assignment was made based on ESI MS and MALDI MS experiments. Clusters were characterized with ^{1}H NMR, 2D NMR, XRD, *etc.* A cluster with same core was synthesized with MPG as a protecting ligand. ESI MS and MALDI MS also confirm the $Ag_{32}MPG_{19}$ composition. Based on NMR investigations, we suggest that most likely the Ag–thiolate is composed of –[S–Ag–S]– motifs. We believe that facile synthesis and the structural insights presented here will stimulate further experimental and theoretical studies on this system.

Acknowledgements

We thank the Department of Science and Technology, Government of India for constantly supporting our research program on nanomaterials. M.S.B. thanks the CSIR for a research fellowship.

References

1 U. Kreibig and M. Vollmer, in *Optical Properties of Metal Clusters*, ed. J. P. Toennies, Springer, Berlin, 1995.
2 L. M. Liz-Marzán, *Langmuir*, 2006, **22**, 32–41.
3 J. Zheng, P. R. Nicovich and R. M. Dickson, *Annu. Rev. Phys. Chem.*, 2007, **58**, 409–431.
4 R. Jin, *Nanoscale*, 2010, **2**, 343–362.
5 T. G. Schaaff, G. Knight, M. N. Shafigullin, R. F. Borkman and R. L. Whetten, *J. Phys. Chem. B*, 1998, **102**, 10643–10646.

6 Y. Negishi, K. Nobusada and T. Tsukuda, *J. Am. Chem. Soc.*, 2005, **127**, 5261–5270.
7 M. A. H. Muhammed, P. K. Verma, S. K. Pal, R. C. A. Kumar, S. Paul, R. V. Omkumar and T. Pradeep, *Chem.–Eur. J.*, 2009, **15**, 10110–10120.
8 E. S. Shibu, M. A. H. Muhammed, T. Tsukuda and T. Pradeep, *J. Phys. Chem. C*, 2008, **112**, 12168–12176.
9 E. S. Shibu and T. Pradeep, *Chem. Mater.*, 2011, **23**, 989–999.
10 A. Ghosh, T. Udayabhaskararao and T. Pradeep, *J. Phys. Chem. Lett.*, 2012, **3**, 1997–2002.
11 E. S. Shibu, B. Radha, P. K. Verma, P. Bhyrappa, G. U. Kulkarni, S. K. Pal and T. Pradeep, *ACS Appl. Mater. Interfaces*, 2009, **1**, 2199–2210.
12 R. Jin, H. Qian, Z. Wu, Y. Zhu, M. Zhu, A. Mohanty and N. Garg, *J. Phys. Chem. Lett.*, 2010, **1**, 2903–2910.
13 H. Qian, Y. Zhu and R. Jin, *J. Am. Chem. Soc.*, 2010, **132**, 4583–4585.
14 H. Qian and R. Jin, *Chem. Commun.*, 2011, **47**, 11462–11464.
15 H. Tsunoyama, Y. Negishi and T. Tsukuda, *J. Am. Chem. Soc.*, 2006, **128**, 6036–6037.
16 Z. Wu, M. A. MacDonald, J. Chen, P. Zhang and R. Jin, *J. Am. Chem. Soc.*, 2011, **133**, 9670–9673.
17 M. Zhu, H. Qian and R. Jin, *J. Am. Chem. Soc.*, 2009, **131**, 7220–7221.
18 M. Zhu, C. M. Aikens, F. J. Hollander, G. C. Schatz and R. Jin, *J. Am. Chem. Soc.*, 2008, **130**, 5883.
19 M. W. Heaven, A. Dass, P. S. White, K. M. Holt and R. W. Murray, *J. Am. Chem. Soc.*, 2008, **130**, 3754–3755.
20 H. Qian, W. T. Eckenhoff, Y. Zhu, T. Pintauer and R. Jin, *J. Am. Chem. Soc.*, 2010, **132**, 8280–8281.
21 C. Zeng, H. Qian, T. Li, G. Li, N. L. Rosi, B. Yoon, R. N. Barnett, R. L. Whetten, U. Landman and R. Jin, *Angew. Chem., Int. Ed.*, 2012, **51**, 13114–13118.
22 P. D. Jadzinsky, G. Calero, C. J. Ackerson, D. A. Bushnell and R. D. Kornberg, *Science*, 2007, **318**, 430–433.
23 Z. Wu, E. Lanni, W. Chen, M. E. Bier, D. Ly and R. Jin, *J. Am. Chem. Soc.*, 2009, **131**, 16672–16674.
24 T. Udayabhaskararao and T. Pradeep, *Angew. Chem., Int. Ed.*, 2010, **49**, 3925–3929.
25 T. Udayabhaskararao, B. Nataraju and T. Pradeep, *J. Am. Chem. Soc.*, 2010, **132**, 16304–16307.
26 M. R. Branham, A. D. Douglas, A. J. Mills, J. B. Tracy, P. S. White and R. W. Murray, *Langmuir*, 2006, **22**, 11376–11383.
27 Y. Negishi, R. Arai, Y. Niihori and T. Tsukuda, *Chem. Commun.*, 2011, **47**, 5693–5695.
28 H. Yang, J. Lei, B. Wu, Y. Wang, M. Zhou, A. Xia, L. Zheng and N. Zheng, *Chem. Commun.*, 2013, **49**, 300–302.
29 H. Yang, Y. Wang and N. Zheng, *Nanoscale*, 2013, **5**, 2674–2677.
30 N. Nishida, H. Yao, T. Ueda, A. Sasaki and K. Kimura, *Chem. Mater.*, 2007, **19**, 2831–2841.
31 S. Kumar, M. D. Bolan and T. P. Bigioni, *J. Am. Chem. Soc.*, 2010, **132**, 13141–13143.
32 O. M. Bakr, V. Amendola, C. M. Aikens, W. Wenseleers, R. Li, L. Dal Negro, G. C. Schatz and F. Stellacci, *Angew. Chem., Int. Ed.*, 2009, **48**, 5921–5926.
33 N. Nishida, H. Yao and K. Kimura, *Langmuir*, 2008, **24**, 2759–2766.
34 N. Cathcart, P. Mistry, C. Makra, B. Pietrobon, N. Coombs, M. Jelokhani-Niaraki and V. Kitaev, *Langmuir*, 2009, **25**, 5840–5846.
35 H. Yao, M. Saeki and K. Kimura, *J. Phys. Chem. C*, 2010, **114**, 15909–15915.
36 K. V. Mrudula, T. Udayabhaskararao and T. Pradeep, *J. Mater. Chem.*, 2009, **19**, 4335–4342.
37 N. Cathcart and V. Kitaev, *J. Phys. Chem. C*, 2010, **114**, 16010–16017.
38 I. Diez and R. H. A. Ras, *Nanoscale*, 2011, **3**, 1963–1970.
39 M. Farrag, M. Thämer, M. Tschurl, T. Bürgi and U. Heiz, *J. Phys. Chem. C*, 2012, **116**, 8034–8043.
40 C. Wang, L. Xu, Y. Wang, D. Zhang, X. Shi, F. Dong, K. Yu, Q. Lin and B. Yang, *Chem.–Asian J.*, 2012, **7**, 1652–1656.
41 A. K. Singh, R. Kanchanapally, Z. Fan, D. Senapati and P. C. Ray, *Chem. Commun.*, 2012, **48**, 9047–9049.
42 B. Adhikari and A. Banerjee, *Chem. Mater.*, 2010, **22**, 4364–4371.
43 J. Guo, S. Kumar, M. Bolan, A. Desireddy, T. P. Bigioni and W. P. Griffith, *Anal. Chem.*, 2012, **84**, 5304–5308.
44 Z. Wu and R. Jin, *Nano Lett.*, 2010, **10**, 2568–2573.
45 H. Hakkinen, M. Walter and H. Grönbeck, *J. Phys. Chem. B*, 2006, **110**, 9927–9931.
46 Z. Wu, C. Gayathri, R. R. Gil and R. Jin, *J. Am. Chem. Soc.*, 2009, **131**, 6535–6542.
47 H. Qian, M. Zhu, C. Gayathri, R. R. Gil and R. Jin, *ACS Nano*, 2011, **5**, 8935–8942.
48 Z. Wu and R. Jin, *ACS Nano*, 2009, **3**, 2036–2042.
49 G. Schmid, *Chem. Soc. Rev.*, 2008, **37**, 1909–1930.
50 H. Xiang, S.-H. Wei and X. Gong, *J. Am. Chem. Soc.*, 2010, **132**, 7355–7360.
51 Y. Sun, K. Balasubramanian, T. Udayabhaskararao and T. Pradeep, *J. Phys. Chem. C*, 2011, **115**, 20380–20387.